In Vitro Biosynthesis of Metal Nanoparticles in Microdroplets

Kyoung G. Lee,[†,¶] Jongin Hong,[‡] Kye Won Wang,[†] Nam Su Heo,[§] Do Hyun Kim,[†] Sang Yup Lee,[†,§] Seok Jae Lee,[¶,*] and Tae Jung Park[§,¶,*]

[†]Department of Chemical & Biomolecular Engineering (BK21) and [§]BioProcess Engineering Research Center, KAIST, 291 Daehak-ro, Yuseong-gu, Daejeon 305-701, Korea, [‡]Department of Chemistry, Chung-Ang University, 84 Heukseok-ro, Dongjak-gu, Seoul 156-756, Korea, and [¶]Center for Nanobio Integration & Convergence Engineering, National Nanofab Center, 291 Daehak-ro, Yuseong-gu, Daejeon 305-806, Korea

ABSTRACT

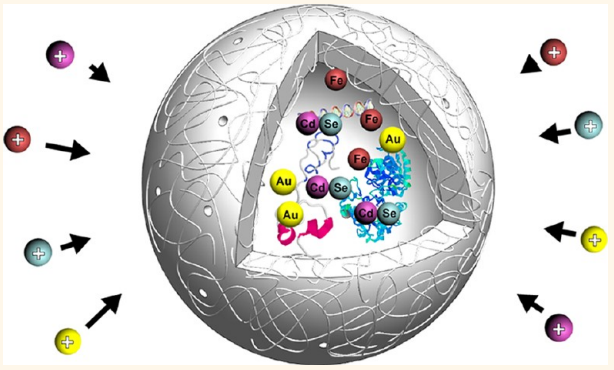

We report the use of a hydrogel polymer, recombinant *Escherichia coli* cell extracts, and a microdroplet-based microfluidic device to fabricate artificial cellular bioreactors which act as reactors to synthesize diverse metal nanoparticles (NPs). The combination of cell extracts, microdroplet-based microfluidic device, and hydrogel was able to produce a mass amount of artificial cellular bioreactors with uniform size and shape. For the first time, we report the alternating generation of microdroplets through one orifice for the fabrication of the artificial cellular reactors using the cell extract as inner cellular components and hydrogel as an artificial cellular membrane. Notably, the hydrogels were able to protect the encapsulated cell extracts from the surrounding environment and maintain the functionality of cellular component for the further cellular bioreactor applications. Furthermore, the successful applications of the fabricated artificial cellular bioreactors to synthesize various NPs including quantum dots, iron, and gold was demonstrated. By employing this microfluidic technique, the artificial cellular bioreactors could be applicable for the synthesis of diverse metal NPs through simple dipping of the reactors to the metal precursor solutions. Thus, the different size of NPs can be synthesized through controlling the concentration of metal precursors. This artificial cellular bioreactors offer promising abilities to biofriendly ways to synthesis diverse NPs and can be applicable in chemical, biomedical, and bioengineering applications.

KEYWORDS: microfluidics · artificial cellular reactor · *in vitro* biosynthesis · metal-binding proteins · nanoparticles

Nanometer-sized colloidal crystals have been explored for diverse applications since their electronic structure and optical and magnetic properties can be fine-tuned by manipulating their physical size. This renders nanoparticles (NPs) ideal materials for bioimaging, therapeutics, catalysis, and optoelectronics.[1−3] However, their synthesis requires sophisticated skills, intuition, and extensive experimentation in order to obtain high-quality NPs that have low defect densities and narrow size distributions. In addition, current synthesis methods of NPs require organic solvents or toxic chemicals, which potentially cause environmental problems. As a result, recent studies have shifted toward alternative synthesis methods, one of which is the *in vivo* synthesis method.[4,5] This *in vivo* synthesis method is to meet the objectives of improved size-selectivity, tighter control over particle properties, and better batch-to-batch reproducibility.[6,7] Park *et al.* recently demonstrated the *in vivo* biosynthesis of diverse NPs including compound semiconductors, magnetic crystals, and noble metals, by constructing recombinant bacteria, *Escherichia coli* strains expressing phytochelatin synthase and metallothionein.[8] The size of NPs was tunable, depending on the concentration of metal ions administered in the medium. However, this reported biosynthesis has a limitation in the usage of precursors and its concentration due to the toxicity against microbial cell growth. Consequently, we herein hypothesize that *in vitro* synthesis of NPs using artificial cellular bioreactors could offer new capabilities to overcome the present limitations.

If metal NPs are to be synthesziedby using artificial cellular bioreactors, following specifics should be satisfied: (1) selection of appropriate materials to produce the artificial cellular structure and (2) production of artificial cellular bioreactors with uniform size and shape. For the first issue, it is essential to accurately understand and mimic natural cellular structures to produce reliable and acceptable artificial cellular bioreactors. The materials to be selected should meet the following qualities: (1) the materials should be biocompatible or at least bioinert; (2) the

* Address correspondence to sjlee@nnfc.re.kr, tjpark@kaist.ac.kr.

Received for review May 8, 2012 and accepted July 6, 2012.

Published online July 09, 2012
10.1021/nn302043q

encapsulated metal-binding proteins in membrane materials should not lose their activity; (3) the metal precursors should be easily diffused into the shell.[9] Until now, liposomes and polymersomes were most closely satisfied with these demands. However, both materials have a critical issue of mechanical and chemical stability in the production of metal NPs. To overcome these issues, hydrogels including poly(*N*-isopropylacrylamide) (PNIPAM),[10] poly(lactic-*co*-glycolic acid) (PLGA),[11] poly(glycerol sebacate) (PGS),[11] poly(ethylene glycol) diacrylate (PEGDA),[12,13] and poly(organophosphazenes)[12] as well as polysaccharides have recently been considered. Among them, PNIPAM, which contains both hydrophilic amide groups and hydrophobic isopropyl groups, is considered highly suitable for the formation of uniform and hollow microgel particles, especially for microfluidics. Importantly, the usage of PNIPAM as an artificial cellular membrane has a great advantage that encapsulants are free from loss of their activities against potential contaminants through bacteria cultivation media. In addition, PNIPAM possesses tiny pores that enable controlled mass transfer of chemical components passing through the membrane during nanoparticle synthesis.[10−15]

For the issue of controlling shape and size of artificial cellular reactors for uniformity, microfluidic techniques have been more extensively employed due to their potential advantages of high-throughput analysis,[16] easy manipulation of fluids and biological components,[17−19] low fabrication cost, and multifunctionality.[20−23] Recently, various types of metal NPs were synthesized by using microfluidic systems or bioengineered cells to overcome the conventional method to fabricate nanomaterials.[24,25] The continuous-flow microfluidic device with a micromixer was used to synthesize cadmium sulfide (CdS), platinum (Pt), palladium (Pd), and CdS core/cadmium selenide (CdSe) shell NPs.[25,26] In nature, cellular organisms, including *Candida glabrata*, engineered *Escherichia coli*, and fungus *Verticillium* sp., are capable of producing several types of metal NPs including CdS, gold (Au), and iron oxide (Fe_3O_4).[26−29] However, in the current microfluidic methods, each precursor should be mixed and introduced at the beginning stage or there should be the merging of two different precursors in microdroplets, which appears limit the production of various types of NPs in a single device simultaneously. In droplet merging-based microfluidic systems, reagents are separately introduced and carefully controlled to be merged with one another to produce the targeted NPs. Unfortunately, this method is unsuitable for mass production or rapid chemical reactions due to the precise control requirements, such as accurate pairing of droplets. Therefore, this type of method is limited to the synthesis of single-type NPs in a single device.

Herein, we developed a new technique for continuous mass production of monodisperse artificial cellular bioreactors made from a hydrogel polymer, cell extracts, and microfluidic device. The cellular components of *E. coli* cells expressing metal-binding proteins were first encapsulated using the microfluidic technique in the *N*-isopropylacrylamide (NIPAM) matrix, and then the NIPAM was polymerized to serve as an individual artificial cellular bioreactor. Such artificial bioreactors can now synthesize various types of NPs since the cellular extracts bind specific metal ions in precursor solutions that are constantly diffused into the reactors. Consequently, the fabricated artificial cellular bioreactors can efficiently encapsulate cellular extracts and serve as individual reactors for *in vitro* biosynthesis of different types of metal NPs.

RESULTS AND DISCUSSION

The primary motivation in this work is to fabricate artificial cellular reactors for the synthesis of different types of metal NPs using hydrogel, microfluidic device, and cell extracts of recombinant *E. coli*. The overall process for the fabrication of artificial cellular bioreactors using a hydrogel polymer, cell extracts, and microfluidic device is schematically illustrated in Figure 1. To verify our proof-of-a-concept constructs, the microfluidic devices were fabricated using soft lithography with poly(dimethylsiloxane) (PDMS; see Figure S1 in Supporting Information for detailed procedure). Next, recombinant *E. coli* cell extracts were encapsulated in NIPAM-based microdroplets and the NIPAM droplets were polymerized (see Figure 1). Importantly, we introduced a new configuration called double-flow focusing to massively and quickly generate NIPAM droplets in the microchannels. In the configuration, two aqueous flows containing the mixture of cell extracts and NIPAM enter to the orifice of a microchannel, and subsequently the droplets are formed by a shearing-off from the oil flows. This new alternative method using oil and water flows leads to ideal one-by-one droplet generation at various flow conditions. Figure 2 shows time-series images of alternating droplet generation in the double flow-focusing configuration. Two immiscible fluids enter the device *via* five parallel microchannels, with the oil phase flowing in the outermost two channels and the central channel and the aqueous phase flowing in each inner channel located between two oil flows. The five liquid streams come into contact just before entering a small orifice (50 μm of width and 110 μm of height) for 2 ms (Figure 2a−e). This contraction leads to the formation of liquid jets in the orifice, and each aqueous jet subsequently breaks into droplets in turn. When a droplet forms in one aqueous jet, the Laplace pressure in the formation of the droplet is decreased as the droplet radius increases. This drives the continuous phase flow backward. Simultaneously, it also generates high resistance to the procession of other flows. After the droplet is pinched off in the orifice, the Laplace pressure changes rapidly, and the retreated aqueous

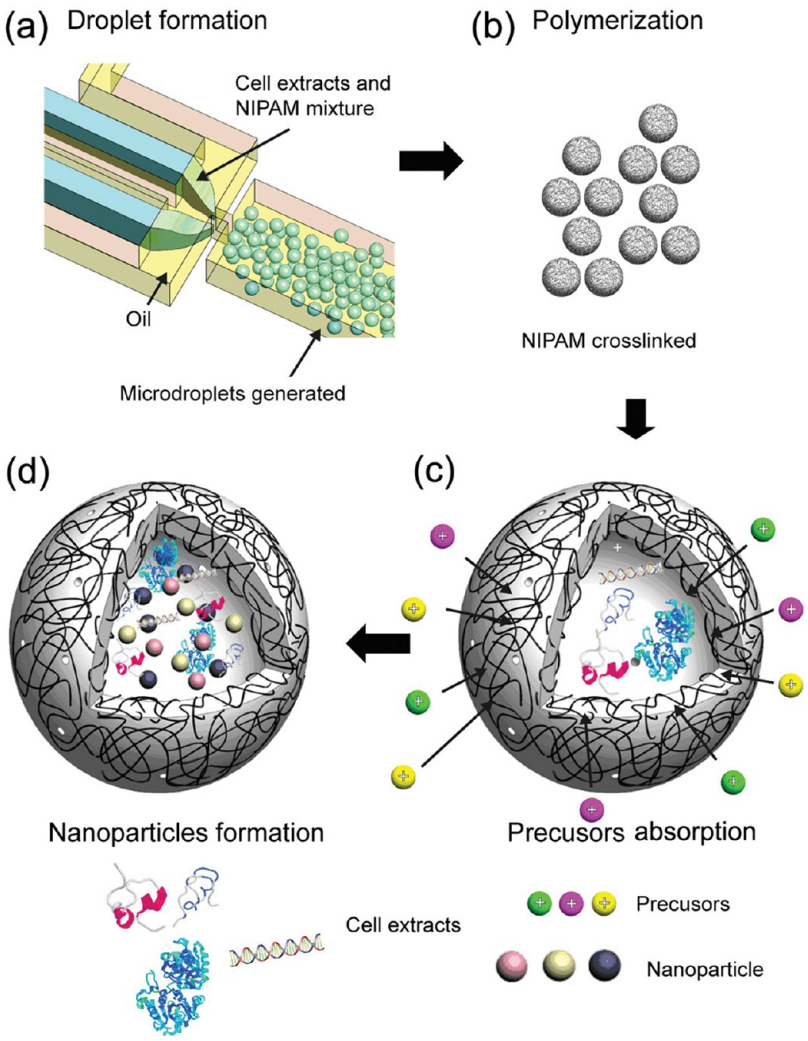

Figure 1. Schematic representation of the microdroplet-generation model using a microfluidic device. (a) Microdroplets are produced with the mixture of cell extracts and NIPAM monomer in a microfluidic device. (b) The polymerized NIPAM monomers serve as an artificial membrane. (c) Different types of precursor solutions are dispersed in the artificial cellular bioreactors. (d) The precursors are transferred into the cells, and NPs are subsequently formed in the artificial cellular bioreactors.

phase retracts to generate a next droplet. This cycle is repeated, and results in strictly alternating droplet production (see Supporting Video S1 and S2). The alternating droplet production in our configuration appears to be similar with two-step emulsification *via* a pressure crosstalk of individual production units except for a moving oil wall.[30−32] Interestingly, three distinct droplet-breakup regimes with different oil flow rates, namely "geometry-controlled" breakup (Figure 2f), "dripping" (Figure 2g−i) and "jetting" (Figure 2j), respectively, were also observed in the double flow-focusing configuration. If the capillary number continues to increase, the aqueous phase fingers extend beyond the exit of the orifice, and form long viscous jets (Figure 2j). Each jet then breaks into individual droplets due to a Rayleigh capillary instability. The droplet size distribution in this mode is not monodisperse, and the droplet generation is less controllable.

The understanding of flow pattern in the microfluidic device is important to control both the reactor size and production rate. For this reason, a confocal microscope and a high-speed camera were used to investigate the flow pattern changes over the different flow rates. The detailed flow pattern was also investigated by confocal microscopy (see Figure S2 in Supporting Information). The upper flow was located at the bottom of the channel, while the other three flows were located at the upper. These asymmetric aqueous flow patterns appeared as flow approached to the orifice (Figure S2b). Both streams generated droplets continuously, and they produced two distinctive layers inside of the microchannels. The surfactant used in this study prevented the aggregation and merging of the newly formed droplets, and this is another key requirement to stably produce the monodisperse artificial cellular bioreactors. Primary droplet sizes in the geometry-controlled regime are roughly equal to the

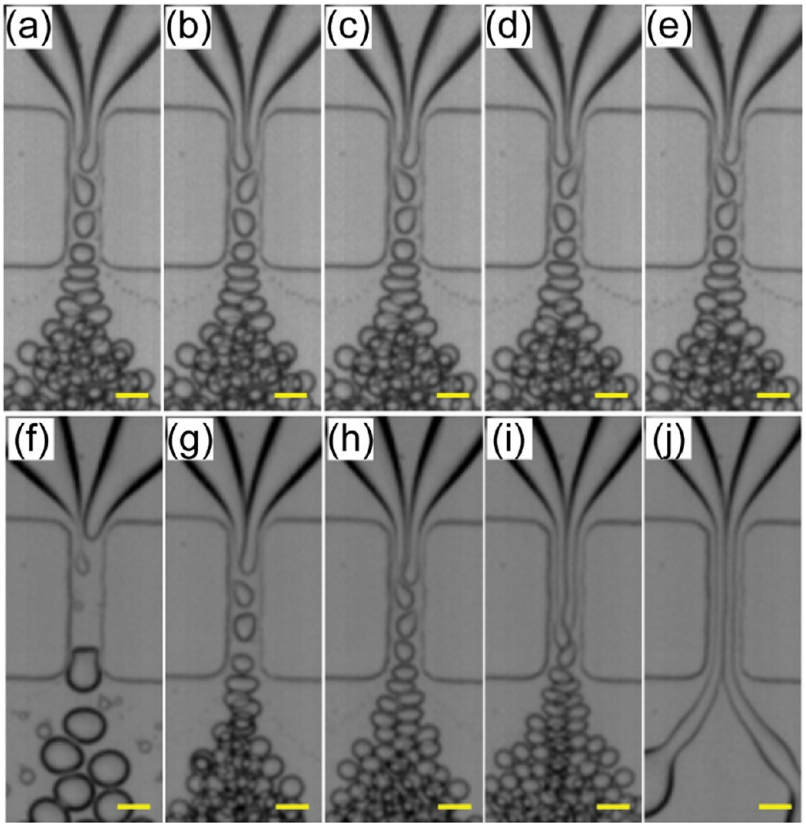

Figure 2. Time-series optical images representing the alternating droplet generation (a–e) and phase diagram for droplet formation in the double flow-focusing configuration (f–j). Droplets are generated at an oil flow of 4.0 μL/min and a polymer flow of 1.5 μL/min: (a) 0, (b) 0.5, (c) 1.0, (d) 1.5, and (e) 2.0 ms, respectively. (f–j) Each image represents the formation of droplet sizes and droplet patterns at an oil flow rate of (f) 2.0, (g) 3.0, (h) 5.0, (i) 7.0, and (j) 8.0 μL/min, respectively, while the ratio of f_{oil} to $f_{polymer}$ is kept constant at 3. Scale bars represent 50 μm.

orifice size, while those in the dripping regime are smaller than the orifice size. In the geometry-controlled regime, a finger of aqueous phase retracts to an upstream position of the orifice after generation of droplets. However, in the dripping regime, the finger remains at a fixed location inside the orifice, even though the droplet is pinched off. Importantly, the transition from the geometry-controlled mode to the dripping mode is related to the increase in the capillary number (*i.e.*, the increase of the oil flow rate in this case). Droplet size distributions in both modes appear to be highly monodisperse, and the droplet size decreases as the capillary number increases. Both droplet size and production frequency in the dripping mode can also be controlled by the change of flow rates in the aqueous phase (see Figure S3 in Supporting Information). Table 1 and Figure S4 (see Supporting Information) show the droplet generation frequencies and average droplet diameters *via* oil flow rates. The size of the microdroplets was measured by optical microscopy. The size of microdroplets can be controlled by changing the flow rate of both continuous and disperse phase solutions. Unlike previous reports that employed *E. coli* or any other microbial cells,[26–29] the size and inner volume of artificial cellular bioreactors can be controlled by changing the flow rates. This controllability means that the inner concentrations of metal binding proteins can also be controlled for biogenic synthesis of metal NPs.

TABLE 1. Summary of Droplet Generation Frequencies and Average Droplet Diameters for Different Oil Flow Rates (μL/min)

	2.0	3.0	5.0	7.0
generation frequency (Hz)	163	1220	2740	4620
average diameter (μm)	54 ± 2.3	34 ± 1.0	29 ± 0.6	26 ± 0.7

The additional polymerization step is required for the fabrication of artificial biocellular reactors after production of microdroplets. There are two common ways to polymerize the monomers: (1) UV polymerization and (2) chemical polymerization. The common method is employing UV light to cross-link the monomers in a short period of time.[32] This method, however, may cause potential damages on cellular components during UV irradiation. For this reason, the chemical polymerization method has been used for cross-linking of the monomer without employing UV light.[13] In chemical polymerization methods, the produced microdroplets should not be merged with one another

for a long period of time, and a sufficient distance should be kept between them. In most cases, it is easy to control the distance between the droplets under their low generation frequency. Unfortunately, it is difficult to control the distance between the droplets under high frequency generation conditions. For this reason, the perfectly separated microdroplets were obtained during the curing process using the microfluidic device by carefully controlling of weight ratio between oil and surfactant (Figure 3a−c and Experimental Section). In this system, two continuous phases never mixed unintentionally during the whole process, and the produced droplets were sterically stabilized among the droplets (see Supporting Video S3) because of the employed surfactant as shown in Figure 3a−c. The employed oil and surfactant (Abil-Em90) mixture produced numerous microdroplets without any fusion during the chemical polymerization because of steric stabilization among droplets (see Figure S5 in Supporting Information).

The production of PNIPAM microdroplets, used as an artificial membrane, was confirmed by employing Fourier transform infrared spectroscopy (FT-IR), which is a powerful tool to identify specific chemical bonds of the surface. To confirm the polymerization of NIPAM, NIPAM monomers and newly obtained PNIPAM microdroplets were analyzed (Figure 3d). The characteristic absorbance bands of NIPAM and PNIPAM are marked with numbers and arrows. The three distinctive absorbance peaks at 917, 965, and 985 cm^{-1} were observed, and these peaks indicate the vibration of the C═C double bond of monomer (NIPAM). After polymerization of NIPAM, the peaks from PNIPAM corresponding to its chemical structure were clearly observed at 1388 cm^{-1} (deformation of methyl group), 1459 cm^{-1} ($-CH_3$ and $-CH_2$ deformation), 1542 cm^{-1} (secondary amide N−H stretching), 1631 cm^{-1} (secondary C═O stretching), 2854 cm^{-1} ($-CH_3$ symmetric stretching), 2929 cm^{-1} (asymmetric $-CH_2$ stretching), 2975 cm^{-1} (asymmetric $-CH_3$ stretching), and 3286 cm^{-1} (secondary amide N−H stretching and bending).[31−33] A comparison of the monomer (NPIAM) and polymer (PNIPAM) shows that the distinct C═C peaks from NIPAM were not observed from the PNIPAM FT-IR spectrum due to the polymerization. Moreover, other major peaks, with the exception of the C═C peaks, were still observed because of the similar chemical structures between NIPAM and PNIPAM (Figure 3d). These results indicated the successful fabrication of an artificial membrane using PNIPAM and a microfluidic device.

To synthesize various types of metal NPs using different types of metal precursors, we adopted this system using cell extracts of recombinant *E. coli*.[8] NIPAM mainly played a role similar to the cellular membrane to protect cellular components from the surrounding environment against losing bioactivities. In addition, the membrane controls the mass transfer rate of metal precursors to synthesize metal NPs inside of droplets. Because of the uniform size and volume of individual droplets, they function as individual chemical reactors and provide unique artificial cellular reactor systems that synthesize various types of metal NPs from different precursor solutions. Importantly, this approach enables us to understand the fabrication mechanisms of inorganic NP-formation using a biotechnological process that does not necessitate complicated tools and expensive raw materials to handle issues of microorganisms' growth and culture contamination. With this rationale in mind, the PNIPAM microdroplets as artificial cellular bioreactors were obtained, and used as individual chemical reactors. More concretely, metal precursor solutions were introduced to the mixture of artificial cellular bioreactors, and transferred into the cells for further reactions. Because of unique characteristics of artificial cellular bioreactors, the kinetics of metal NP-formation provides highly similar morphology in all droplets throughout the whole experiment. It has been confirmed that an individual microdroplet functions as a simple chemical reactor to synthesize metal NPs.

As previously discussed, the artificial cellular reactors were successfully fabricated and conserved the cell extracts for using as the artificial cellular bioreactors. To confirm feasibility of the constructed artificial cellular bioreactor for the fabrication of metal NPs, we performed metal uptake studies for the three different metals including Fe, Cd/Se, and Au precursors. These three different precursors were selected as representative examples to demonstrate metal oxide NPs, metal alloy NPs, and size controllability of NPs, respectively. Furthermore, these three different types of NPs are popular to researchers due to the high demands and variety applications from last few decades. The NPs formation process and types of precursors are demonstrated in Figure S6 and Table S1 (see Supporting Information), respectively. The Fe and Cd/Se metal precursors were dissolved in deionized (DI) water and added to the reactor mixture solution with 5 mM concentrations. To determine the synthesis of different types of NPs, we used field emission transmission electron microscopy (FE-TEM).

As an example for the synthesis of pure metal oxide NPs, we selected Fe NPs for further demonstration. The average size of synthesized Fe_3O_4 NPs that show the crystalline structures with a specific interplanar lattice distance of 2.53 $\pm$ 0.51 Å in the {311} cubic structure, is 4.42 $\pm$ 1.58 nm (Figure 4a−4c).[34] The chemical elements of NPs were analyzed by energy-dispersive X-ray spectroscopy (EDAX) as shown in Figure 4d. Moreover, the color change of artificial cellular bioreactors was also shown in Figure S7 (see Supporting Information). These results indicate the successful synthesis of Fe magnetic NPs in the bioreactors. Before Fe precursors were introduced to the reactor mixture solution, the

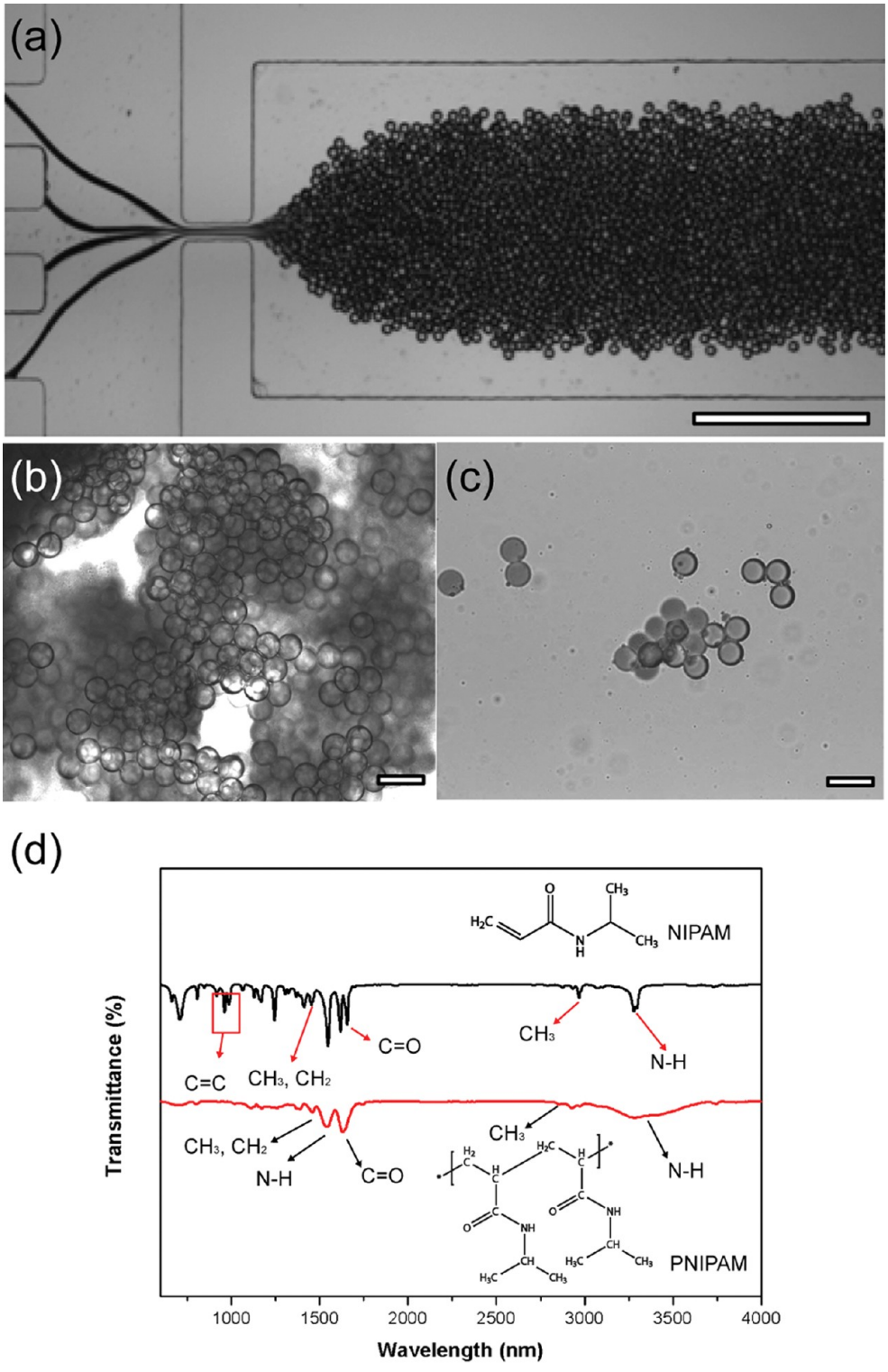

Figure 3. (a) Optical microscopic images of double flow-focusing to generate droplets (artificial cellular bioreactors) suspended (b) in oil and (c) in water (scale bars represent 100 μm). (d) FT-IR spectra of monomer (NIPAM) and polymerized microdrobeads (PNIPAM) using microfluidic device.

reactors showed white color. As the Fe precursor solution was injected into the reactor, the color of reactors was converted from white to orange as shown in Figure S7. These results indicate the successful synthesis of Fe magnetic NPs in the bioreactors.

In the synthesis of metal alloy NPs, quantum dots (QDs) is a good candidate for the demonstration. For this reason, we selected CdSe QDs as a representative material of QDs and the 5 mM of each Cd and Se precursors were applied to the artificial cellular

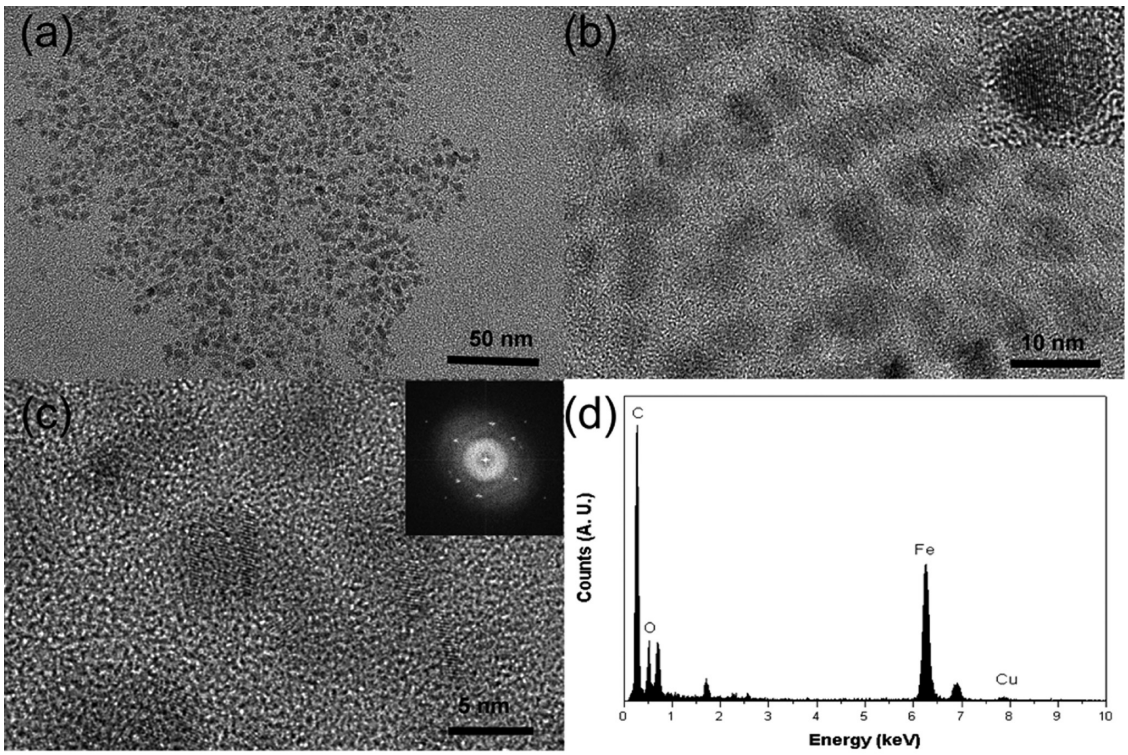

Figure 4. TEM images of (a) low resolution of Fe_3O_4, NPs and (b-c) high resolution-TEM image of Fe_3O_4 NPs. The inserted HR-TEM image represents diffraction images from its HR-TEM data. (d) EDAX data for the Fe_3O_4 NPs.

bioreactors. As we expected, the strong red fluorescent signal from QDs was observed from inside of the artificial cellular reactors by using a confocal microscopy (Figure 5a−5c). Furthermore, the morphology of QDs was investigated using TEM as shown in Figure 5d and Supporting Information Figure S8. The average diameter of CdSe QDs was 5.00 ± 0.79 nm, and the NPs showed well-defined crystalline structures with specific interplanar lattice distances of 3.72 ± 0.73 and 3.51 ± 0.49 Å lattice structures, which represent {100} hexagonal and {111} cubic structures, respectively.[34] The chemical elements of synthesized QDs were composed of Cd and Se which were confirmed by EDAX analysis (Figure 5e). For the further verification of CdSe QDs using the artificial cellular bioreactors, the optical properties were investigated using both photoluminescence spectroscopy and ultraviolet−visible (UV−vis) spectroscopy. The synthesized QDs exhibited an absorption shoulder around 380 nm and emission peak around 710 nm (Figure 5f). On the basis of the data, the CdSe QDs were successfully synthesized using the artificial cellular bioreactors.

The Fe and CdSe NPs were selected to demonstrate the successful synthesis of pure metal oxide NPs and metal alloy NPs using the artificial cellular bioreactors. We also selected Au NPs as an example to show the size controllability of NPs using the artificial cellular bioreactors. To test the size control of Au NPs, five different concentrations of Au precursor solution (5, 10, 20, 30, and 50 mM, respectively) were applied into the artificial cellular bioreactors. The size-dependent features of the as-synthesized Au NPs were verified by their TEM images (Figure 6a−e and Supporting Information Figures S9−S13). For the further verification of Au NPs, the synthesized Au NPs were analyzed by EDAX, and the formation of Au NPs in the reactors was confirmed as shown in Supporting Information Figure S14. At the concentration of Au NPs below 50 mM, the morphology of NPs showed either spherical or ellipsoidal shapes. In the case of 50 mM precursor solution, the formation of Au NPs with irregular shapes was observed (see Figure S13 in Supporting Information). After the incubation with corresponding Au precursor solutions, the size changes of Au NPs in the artificial cells were analyzed through wavelength shifts by UV−vis spectrometry and optical color changes by the naked-eye (Figure 6f). After placing the artificial cellular bioreactors in 5−50 mM of Au precursor solution, the white color of the bioreactors turned into bright pink, purple, and deep purple colors with different concentrations. Moreover, the optical properties of the bioreactors were changed over the different concentrations of Au precursors as observed using UV−vis spectroscopy as shown in Figure 6g. The absorbance changes also supported the particle differences in the bioreactors as shown in Figure 6g. Furthermore, the size changes of the Au NPs were also confirmed by measurement of the Au NPs using TEM images. The overall size changes were summarized and are shown in Figure 6h, and the size distribution of Au

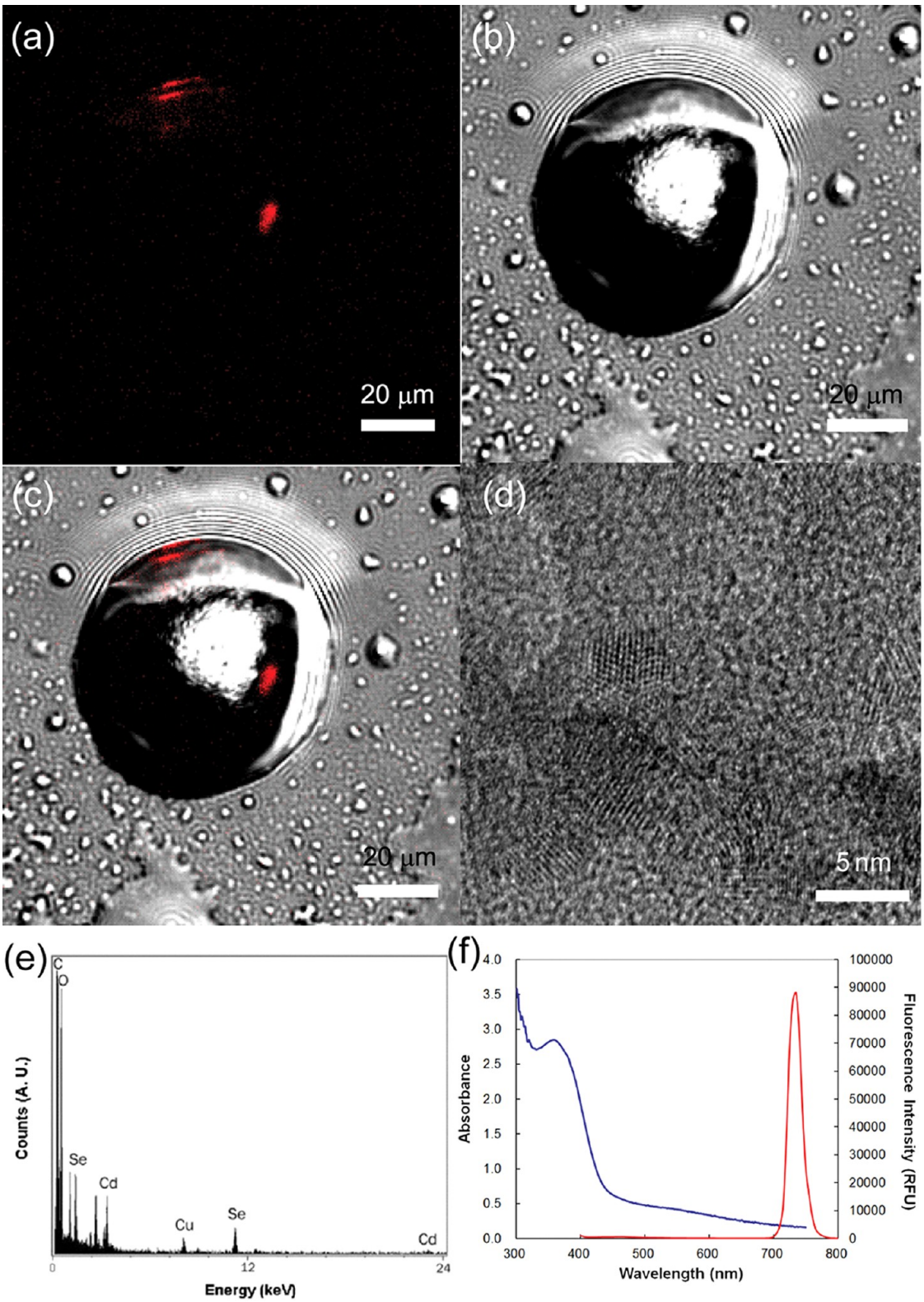

Figure 5. (a) Fluorescent image of CdSe QDs in the artificial cellular bioreactor. (b) Optical microscopic image of the artificial cellular bioreactor. (c) Overlap of fluorescent CdSe QDs and optical image of the artificial cell. (d) TEM image of CdSe QDs in the artificial cellular bioreactor. (e) EDAX data for the CdSe QDs. (f) UV−vis (blue line) and fluorescent emission (red line) spectroscopies of the CdSe QDs.

NPs is shown in Supporting Information Figure S15. In addition, most of the synthesized Au NPs show crystalline structures with a specific interplanar lattice distance of 2.35 ± 0.12 Å with {111} cubic structure

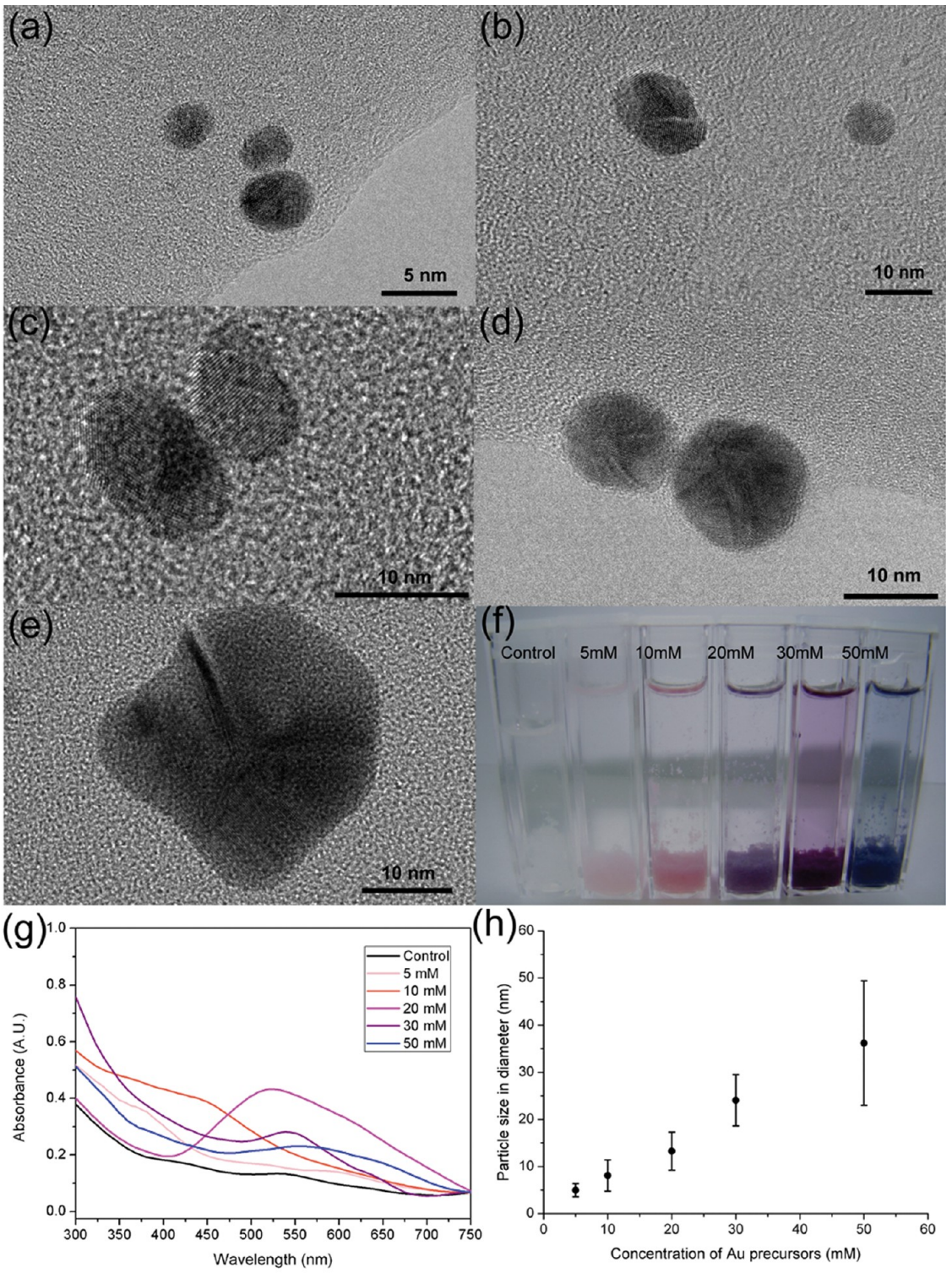

Figure 6. TEM images of Au NPs with different precursor concentrations of (a) 5, (b) 10, (c) 20, (d) 30, and (e) 50 mM, respectively. (f) Picture of the different concentrations of Au NPs in the artificial cellular bioreactors. (g) UV–vis spectra of different concentrations of Au NPs in the artificial cellular bioreactors. (h) Average particle sizes and standard deviations of Au NPs corresponding to the precursor concentrations in the artificial cellular bioreactors. The sizes were determined by measurements at least 100 particles from obtained TEM images.

which was commonly observed in the synthesized Au NPs.

Finally, chemical compositions of synthesized metal NPs using the artificial cellular bioreactors were confirmed and properly matched to the metal elements by EDAX analysis. Taken together, simple *in vitro* metal biosynthesis of CdSe, Fe, and Au NPs was successfully developed with size-tunability and metal

selectivity by using a chemical reactor system in microdroplets as artificial cells.

CONCLUSION

We demonstrated the *in vitro* synthesis of various types of metal NPs using the artificial cellular bioreactors that served as individual biofactories. The artificial cellular bioreactors were successfully fabricated using the combination of microfluidic and bioengineering techniques. The size of artificial cellular bioreactors was controlled to be between 26 to 53 μm by varying the flow rate of both continuous and disperse phases in microfluidic channels. These microdroplets can be directly manipulated with microfluidic design to control their size and volume. Accordingly, three different types of metal NPs including QD, magnetic particle, and noble crystal were successfully synthesized inside of the artificial cellular bioreactors by passing through the artificial membrane while simultaneously importing metal precursors. As a conclusion, the on-chip-synthesized artificial cellular bioreactor system effectively functions as an individual chemical reactor to synthesize different types of metal nanocomposite materials with high biocompatibility, and to preserve the bioactivity. In addition, the microfluidic technique provides a unique condition to produce monodisperse microdroplets with easy control of the concentration of cellular components, in contrast to real living cells. We believe that this biomimetics is a powerful method for the biosynthesis of various metal NPs with the use of cellular behavior and a metal growing mechanism. Moreover, it is believed that our double flow-focusing method is highly applicable to fabricating artificial cells, thereby enhancing our understanding of the cellular detoxification mechanisms.[35,36]

EXPERIMENTAL SECTION

Materials. *N*-Isopropylacrylamide (NIPAM), *N*-*N*′-methylenebisacrylamide (BIS, cross-linker), ammonium persulphate (APS), D-sorbitol, *N*,*N*,*N*,*N*′-tetramethylethylenediamine (TEMED, 99.9%), isopropyl alcohol (IPA, 99.9%), and phosphate-buffered saline (PBS) were purchased from Sigma-Aldrich. The SU-8 photoresist and developer solution were purchased from Microchem. The polydimethylsiloxane (PDMS) was obtained from Dow Corning. Refined grape-seed oil (G-oil, Beksul) and Abil-EM90 (Degussa) as a surfactant were mixed, and used as a continuous flow solution.

Microfabrication of the Microfluidic Device. The silicon master was fabricated with SU-8 photoresist using photolithography of a PDMS molding technique. Microfluidic devices were obtained with PDMS using a silicon master with SU-8 pattern. A mixture of PDMS prepolymer and curing agent (10:1 Sylgard184, Dow Corning) was stirred and degassed in a vacuum oven at 70 °C. After curing, the PDMS replica was peeled away from the silicon master, and then bonded with another PDMS using O_2 plasma.

Droplet Polymerization. The droplets were generated using a microfluidic device with a modified flow-focusing technique. The droplet polymerization (DP) was prepared from the mixture of potassium persulfate (initiator, 0.19 wt %), BIS (cross-linker, 0.6 wt %), DI water (56 wt %), NIPAM (24.8 wt %), and cell extract and PBS solution (0.18 wt %). The continuous phase is the mixture solution of G-oil and Abil-EM90 (2 wt %). The generation of microdroplets as artificial cells in the microfluidic device was observed using an optical microscope with a charge-coupled-device camera (Elipse Ti−S, Nickon) and a high speed camera (Phantom V7.3, Vision Research Inc., USA). Once the microdroplets were generated through the orifice using a modified flow-focusing technique, the droplets were collected and suspended in TEMED/G-oil mixture (25 wt %) for the polymerization. TEMED acts as a promoter for accelerating the polymerization and producing hydrogels. In addition, the Abil-EM90, silicone emulsifier, prevents the coagulation among the produced droplets due to steric stabilization during the polymerization. The polymerized microdroplets were washed with IPA and PBS solution several times, and then dispersed in different metal precursor solutions.

Instrumentation. A high speed camera was used to record the passage of multiple droplets at 50 000 frames per second. An image processing algorithm was modified to analyze recorded images in this study.[1] The microdroplet generation movies were also taken by a high speed camera. The morphology of metal NPs was investigated using the field emission scanning electron microscopy (FE-SEM, Hitachi S4800) and the field emission transmission electron microscopy (FE-TEM, JEOL JEM-2100F). The microdroplets generation in the microfluidic device was observed using an optical microscope with a charge-coupled-device camera. A UV−vis spectrometer (Optizen 3220UV, Mecasys, Korea) was used for analysis of synthesized Au NPs in the hydrogel and CdSe QDs. The photoluminescence spectrometer (SpectraMax M2, Molecular Devices) was employed to investigate the luminescent property of CdSe QDs.

Conflict of Interest: The authors declare no competing financial interest.

Acknowledgment. This research was supported by the HTS-based Integrated Technology Development Grant 2008-04171 from the Korea Ministry of Education, Science and Technology (KMEST) and the Technology Innovation Program through the Korea Innovation Cluster Foundation funded by the Ministry of Knowledge Economy (No. A2010D-D013). Additional support was provided by the Project for Developing Systems Metabolic Engineering Platform Technologies for Biorefineries, Technology Development Program to Solve Climate Changes (NRF-2012-C1AAA001-2012M1A2A2026556), and from the KMEST through the National Research Foundation. We also thank H.-W. Choi (NNFC) for assistance with graphic illustrations.

Supporting Information Available: Detailed dimensions of the microfluidic device; the flow pattern for the production of microdroplets analyzed using a fluorescent dye, a confocal microscopy, and a high-speed camera; schematic illustration of the formation mechanism of metal NPs; TEM and EDAX analysis of the CdSe QDs and Au NPs; table listing the metal precursors. This material is available free of charge *via* the Internet at http://pubs.acs.org.

REFERENCES AND NOTES

1. Xia, Y.; Xiong, Y.; Lim, B.; Skrabalak, S. E. Shape-Controlled Synthesis of Metal Nanocrystals: Simple Chemistry Meets Complex Physics. *Angew. Chem., Int. Ed.* **2009**, *48*, 60–103.
2. Lee, K. G.; Wi, R.; Park, T. J.; Yoon, S. H.; Lee, J. B.; Lee, S. J.; Kim, D. H. Synthesis and Characterization of Gold-Deposited Red, Green and Blue Fluorescent Silica Nanoparticles for Biosensor Application. *Chem. Commun.* **2010**, *46*, 6374–6376.
3. Piao, Y.; Kim, J.; Na, H. B.; Kim, D.; Baek, J. S.; Ko, M. K.; Lee, J. H.; Shokouhimehr, M.; Hyeon, T. Wrap-Bake-Peel Process for Nanostructural Transformation from beta-FeOOH Nanorods to Biocompatible Iron Oxide Nanocapsules. *Nat. Mater.* **2008**, *7*, 242–247.

4. Dameron, C. T.; Reese, R. N.; Mehra, R. K.; Kortan, A. R.; Carroll, P. J.; Steigerwald, M. L.; Brus, L. E.; Winge, D. R. Biosynthesis of Cadmium Sulphide Quantum Semiconductor Crystallites. *Nature* **1989**, *338*, 596–597.
5. Kang, S. H.; Bozhilov, K. N.; Myung, N. V.; Mulchandani, A.; Chen, W. Microbial Synthesis of CdS Nanocrystals in Genetically Engineered *E. coli*. *Angew. Chem., Int. Ed.* **2008**, *47*, 5186–5189.
6. Discher, D. E.; Eisenberg, A. Polymer Vesicles. *Science* **2002**, *297*, 967–973.
7. Tanaka, M.; Sackmann, E. Polymer-Supported Membranes as Models of the Cell Surface. *Nature* **2005**, *437*, 656–663.
8. Park, T. J.; Lee, S. Y.; Heo, N. S.; Seo, T. S. *In Vivo* Synthesis of Diverse Metal Nanoparticles by Recombinant *Escherichia coli*. *Angew. Chem., Int. Ed.* **2010**, *49*, 7019–7024.
9. Lutolf, M. P.; Hubbell, J. A. Synthetic Biomaterials as Instructive Extracellular Microenvironments for Morphogenesis in Tissue Engineering. *Nat. Biotechnol.* **2005**, *23*, 47–55.
10. You, Y.; Kalebaila, K. K.; Brock, S. L.; Oupicky, D. Temperature-Controlled Uptake and Release in PNIPAM-Modified Porous Silica Nanoparticles. *Chem. Mater.* **2008**, *20*, 3354–3359.
11. Ling, Y.; Rubin, J.; Deng, Y.; Huang, C.; Demirci, U.; Karp, J.; Khademhosseini, A. A Cell-Laden Microfluidic Hydrogel. *Lab Chip* **2007**, *7*, 756–762.
12. Nayak, S.; Lyon, L. A. Soft Nanotechnology with Soft Nanoparticles. *Angew. Chem., Int. Ed.* **2005**, *44*, 7686–7708.
13. Lee, K. G.; Park, T. J.; Soo, S. Y.; Wang, K. W.; Kim, B. I.; Park, J. H.; Lee, C.; Kim, D. H.; Lee, S. J. Synthesis and Utilization of *E. coli*-Encapsulated PEG-Based Microdroplet Using a Microfluidic Chip for Biological Application. *Biotechnol. Bioeng.* **2010**, *107*, 747–751.
14. Chen, Z.; Xu, L.; Liang, Y.; Zhao, M. pH-Sensitive Water-Soluble Nanospheric Imprinted Hydrogels Prepared as Horseradish Peroxidase Mimetic Enzymes. *Adv. Mater.* **2010**, *22*, 1488–1492.
15. Calvert, P. Hydrogels for Soft Machines. *Adv. Mater.* **2009**, *21*, 743–756.
16. Song, H.; Chen, D. L.; Ismagilov, R. F. Reaction in Droplets in Microfluidic Channels. *Angew. Chem., Int. Ed.* **2006**, *45*, 7336–7356.
17. Valencia, P. M.; Basto, P.; Zhang, A.; Rhee, L.; Langer., M.; Farokhzad, R.; Karnik, O. C.; Single-Step, R. Assembly of Homogenous Lipid-Polymeric and Lipid-Quantum Dot Nanoparticles Enabled by Microfluidic Rapid Mixing. *ACS Nano* **2010**, *4*, 1671–1679.
18. Hu, M.; Yan, J.; He, Yao; Lu, H.; Weng, L.; Song, S.; Fan, C.; Wang, L. Ultrasensitive, Multiplexed Detection of Cancer Biomarkers Directly in Serum by Using a Quantum Dot-Based Microfluidic Protein Chip. *ACS Nano* **2010**, *4*, 488–494.
19. Hong, J.; Edel, J. B.; deMello, A. J. Micro-and Nanofluidic Systems for High-Throughput Biological Screening. *Drug Discovery Today* **2009**, *14*, 134–146.
20. Srisa-Art, M.; Kang, D. K.; Hong, J.; Park, H.; Leatherbarrow, R. J.; Edel, J. B.; Chang, S.-I.; deMello, A. J. Analysis of Protein−Protein Interactions by Using Droplet-Based Microfluidics. *ChemBioChem* **2009**, *10*, 1605–1611.
21. Wang, G.; Lim, C.; Chen, L.; Chon, H.; Choo, H.; Hong, J.; deMello, A. J. Surface-Enhanced Raman Scattering in Nanoliter Droplets: Towards High-Sensitivity Detection of Mercury (II) Ions. *Anal. Bioanal. Chem.* **2009**, *394*, 1827–1832.
22. Hong, J.; Choi, M.; deMello, A. J.; Edel, J. B. Interfacial Tension-Mediated Droplet Fusion in Rectangular Microchannels. *BioChip J.* **2009**, *3*, 203–207.
23. Chu, L.-Y.; Utada, A. S.; Shah, R. K.; Kim, J.-W.; Weitz, D. A. Controllable Monodisperse Multiple Emulsions. *Angew. Chem., Int. Ed.* **2007**, *46*, 8970–8974.
24. Whitesides, G. M. The Origins and the Future of Microfluidics. *Nature* **2006**, *442*, 368–373.
25. Teh, S. Y.; Lin, R.; Hung, L.; Lee, A. P. Droplet Microfluidics. *Lab Chip* **2008**, *8*, 198–220.
26. Kang, S. H.; Bozhilov, K. N.; Myung, N. V.; Mulchandani, A.; Chen, W. Microbial Synthesis of CdS Nanocrystals in Genetically Engineered *E. coli*. *Angew. Chem., Int. Ed.* **2008**, *47*, 5186–5189.
27. Dameron, C. T.; Smith, B. R.; Winge, D. R. Glutathione-Coated Cadmium-Sulfide Crystallites in *Candida glabrata*. *J. Biol. Chem.* **1989**, *264*, 17355–17360.
28. Mukherjee, P.; Ahmad, A.; Mandal, D.; Senapati, S.; Sainkar, S. R.; Khan, M. I.; Ramani, R.; Parischa, R.; Ajayakumar, P. V.; Alam, M.; *et al.* Bioreduction of $AuCl_4^-$ Ions by the Fungus *Verticillium* sp. and Surface Trapping of the Gold Nanoparticles Formed. *Angew. Chem., Int. Ed.* **2001**, *40*, 3585–3588.
29. Philipse, A. P.; Maas, D. Magnetic Colloids from Magnetotactic Bacteria: Chain Formation and Colloidal Stability. *Langmuir* **2002**, *18*, 9977–9984.
30. Song, Y.; Hormes, J.; Kumar, C. S. S. R. Microfluidic Synthesis of Nanomaterials. *Small* **2008**, *4*, 698–711.
31. Chokkalingam, V.; Herminghaus, S.; Seemann, R. Self-Synchronizing Pairwise Production of Monodisperse Droplets by Microfluidic Step Emulsification. *Appl. Phys. Lett.* **2008**, *93*, 254101–254103.
32. Okushima, S.; Nisisako, T.; Torii, T.; Higuchi, T. Controlled Monodispersed Double Emulsions by Two-Step Droplet Breakup in Microfluidic Device. *Langmuir* **2004**, *20*, 9905–9908.
33. Choi, C.; Jung, J.; Kim, D.; Chung, Y.; Lee, C. Novel One-Pot Route to Monodisperse Thermosensitive Hollow Microcapsules in a Microfluidic System. *Lab Chip* **2008**, *8*, 1544–1551.
34. *Powder Diffraction Data File 38-1364, Inorganic Phases*; JCPDS International Centre for Diffraction Data: Swathmore, PA, 1990.
35. Shahverdi, A. R.; Minaeian, S.; Shahverdi, H. R.; Jamalifar, H.; Nohi, A. Rapid Synthesis of Silver Nanoparticles Using Culture Supernatants of Enterobacteria: A Novel Biological Approaches. *Process Biochem.* **2007**, *42*, 919–923.
36. Labrenz, M.; Druschel, G. K.; Thomsen-Ebert, T.; Gilbert, B.; Welch, S. A.; Kemner, K. M.; Logan, G. A.; Summons, R. E.; Stasio, G. D.; Bond, P. L.; *et al.* Formation of Sphalerite (ZnS) Deposits in Natural Biofilms of Sulfate-Reducing Bacteria. *Science* **2000**, *290*, 1744–1747.